J Mater Sci (2007) 42:4545–4551
DOI 10.1007/s10853-006-0482-0

Metal–ceramic composite layers on stainless steel through the combination of electrophoretic deposition and galvanic processes

A. Knote · H. G. Krüger · S. Selve · Th. Kups · H. Kern · L. Spiess

Received: 5 January 2006 / Accepted: 31 May 2006 / Published online: 16 February 2007

Abstract The use of metal–ceramic composite layers is of considerable technical interest for many areas of application. The use of electrochemical processes makes it possible to realize coatings on stainless steel which combine the properties of the metals with those of ceramics in an outstanding manner. The process presented here is based on a combination of electrophoretic and electrolytic deposition. At the same time, a very high ceramic ratio is attained in comparison to electrolytic dispersion depositions. It was therefore possible to achieve both nickel–zirconium oxide as well as a copper–zirconium oxide coatings with strong adhesive bonds on stainless steel. A preliminary nickel plating or preliminary copper plating of the stainless steel substrate was first realized. A nanoscale zirconium oxide powder (Tosoh TZ-8Y) from an ethanolic suspension was then applied electrophoretically onto this layer and sintered to an open-porous layer with a porosity of 40–50%. After this, the metal was galvanically infiltrated into the pores. An annealing process was then carried out to improve the layer bonding. Solid-state physical tests reveal that a good material bonding of the composite layer onto the substrate occurred as a result of diffusion processes. Metal–ceramic composite layers can be produced through a combination of electrophoretic and electroplating technology with strongly bond on the substrate by a final heat treatment.

A. Knote · H. G. Krüger · H. Kern
Department of Materials Engineering, Technical University Ilmenau, 98693 Ilmenau, Germany

S. Selve · Th. Kups · L. Spiess (✉)
Center for Micro and Nanotechnologies,
Technical University Ilmenau, 98693 Ilmenau, Germany
e-mail: lothar.spiess@tu-ilmenau.de

Introduction

There is a continuous need for coated metallic components, e.g. for wear and corrosion protection, as well as for applications at high temperatures. These coatings are expected to exhibit both a high wear and corrosion resistance as well as a good adhesive bonding to the metallic component, excellent thermal shock resistance and high damage tolerance during mechanical stress.

As an alternative to the pure ceramic coatings, attempts have been made to develop metal–ceramic composite layers in which the favorable properties of metals, for example ductility, can be combined with the hardness and wear-resistance of ceramics. These processes include, for example, electrolytic dispersion deposition, in which small ceramic particles are dispersed in the electrolytes and deposited together with the metal [1, 2]. Dispersion composite coatings with nanoscale ceramic powders hold promise, above all, of a significant increase in the hardness, wear resistance and maximum application temperature [3, 4]. However, the high specific surface of fine ceramic particles and the tendency associated with this to form particle agglomerates only allow low particle concentrations. Values of up to 11 vol% are normally cited in the relevant literature, i.e. the properties of the electrolytically deposited metal dominate in these coatings [3, 4].

Other options for producing metal–ceramic composite layers are the co-deposition of ceramic and metal particles and the deposition of metal-coated ceramic particles by means of electrophoresis [5, 6]. A subsequent sintering process enables the ceramic particles to be integrated in the metallic matrix.

Current studies focus on a combination of electrophoretic deposition and electroplating technology. These are characterized in such way that the electrophoretic and galvanic coatings are realized one after the other, whereby however thermal intermediate stages are necessary [7–10]. In previous investigations it was found that in both these stages, however, no sufficient adhesive bonding was achieved. In the present study an improvement of the method has been developed. It is based on the application of a metal intermediate coating galvanically onto the metal substrate for improvement of the coating adhesive bond.

Experimental methods

Materials and processing

The tests were carried out on stainless steel X6Cr17 (AISI 430) in dimensions of 40 × 25 mm^2. For production of the metal–ceramic composite layers, the metal substrate was first degreased and then electroplated with a thin metal layer (5–10 μm). Figure 1 shows a schematic diagram of the deposition cell, where all electrophoretic deposition (EPD) processes were done. For this process, the substrate surface was first activated and roughened in a preliminary nickel-plating bath. The metal intermediate layer was then applied either from a nickel sulfamate electrolyte, which is characterized by its low internal voltages, or from an acid copper electrolyte, shown in Table 1.

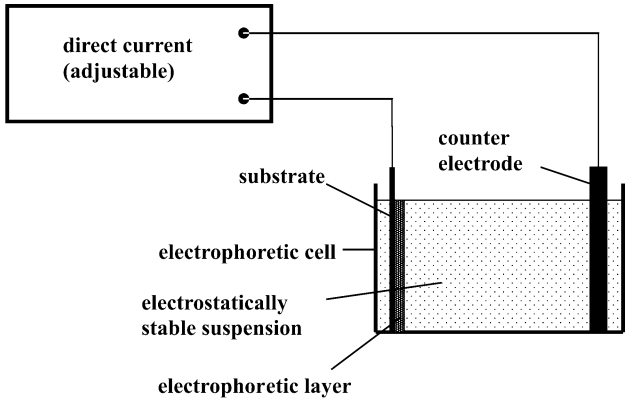

Fig. 1 Schematic diagram of the electrophoretic deposition cell

The ceramic powder used was zirconium oxide TZ-8Y fully stabilized with yttrium oxide (Tosoh Corporation, Japan) with an average primary particle size of approx. 45 nm. The material were supplied as a spray-dried granulate with a particle size of approx. 60 μm. This powder was electrophoretically applied onto this primary electroplating coating. For this, it is necessary to prepare the fine powder into an agglomerate-free, electrostatically stable suspension.

The zirconium oxide powder was dispersed ultrasonically with the addition of 4-hydroxybenzoic acid in ethanol and a small part of water. An alcoholic dispersion is to be preferred rather than water, as gas bubble formation or passivation of the metal surface as a result of electrolysis cannot be excluded during a direct electrophoretic coating of metals. The 4-hydroxybenzoic acid served as a dispersant and binder at the same time. A suspension consisting of 100 g ZrO_2 powder + 100 g ethanol + 6 g de-ionized water + 4 g 4-hydroxybenzoic acid was used for the tests. The electrophoretic deposition were realized at current densities of 0.2–2 mA/cm^2 with 2–5 s coating time.

After drying in air, the layer was sintered for 3 h in vacuum at temperatures of 1050–1150 °C (heating rate: 570 K/h; cooling rate: 150 K/h). An open-porous layer of ~50% porosity was formed.

After this process, the open porosity in the ceramic layer was galvanically filled with metal. The same electrolytes used to apply the metallic intermediate

Table 1 Composition of the metal electrolytes used and deposition parameters

	Preliminary nickel plating	Nickel sulfamate electrolyte	Acid copper electrolyte
Composition	200 g/l nickel chloride × 6 H_2O, 60 ml/l hydrochloric acid	600 g/l nickel sulfamate × 4 H_2O, 40 g/l boric acid, 5 g/l nickel chloride × 6 H_2O	250 g/l copper sulfate × 5 H_2O, 50 ml/l conc. sulfuric acid, 80 mg/l sodium chloride
Working temperature	20 °C	55 °C	20 °C
Anode	Nickel	Depolarized nickel	Copper
Current density	3 A/dm^2	5 A/dm^2	4 A/dm^2
Deposition time	2 min anodic, 6 min cathodic	9 min	5 min
Electrode spacing	3 cm		

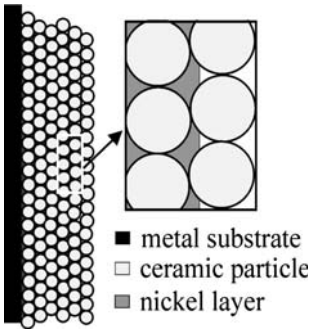

Fig. 2 Infiltration of the open porosity in the zirconium layer with nickel (schematic representation)

layer were employed. For this process it was important for the current density to be halved in relation to the entire sample area, as a part of the metal substrate was covered by the ceramic layer at a porosity of 50%. As schematically shown in Fig. 2 the metal penetrates the pores, starting from the substrate or the first metallic layer, and then completely fills these.

A final heat treatment of 1 h at 800 °C in vacuum then enabled the good bonding of the composite layer onto the substrate via diffusion processes.

Characterization

The characteristics of the initial powder was ascertained by TEM. The metal infiltration in the pores was demonstrated both by TEM/EELS as well as EDX tests. The microstructure of the layers was examined using X-ray diffractometry and scanning electron microscopy (SE and BSE mode). The strong bonding through diffusion of the coating components was confirmed through EDX line scans. Roughness was measured by profilometer form talysurf series 2 (Taylor Hobson). The cut off of the measurement was 0.8 mm. The porosity was indirectly calculated from SEM images.

The layer thicknesses were measured after drying the layer via profile measurements using a tracing stylus instrument (Taylor Hobson). For this, a part of the green layer was removed and the height difference measured between the layer surface and the metal substrate. Besides the reduced effort for sample preparation, this process ensures a more accurate determination of the layer thickness in comparison to other measuring methods.

Results and discussion

The substrate surface was activated for electrolytic deposition as a result of the preliminary nickel plating. The metal substrate was also rendered rougher. The adhesion of the galvanic layer on the substrate was thereby improved. This proved to be advantageous for the copper layer as well. The average roughness R_a considerably increased on account of the preliminary nickel plating (Table 2). While no significant differences in the roughness values were observed in the untreated sample depending on the rolling direction of the metal substrate, these become discernible, however, after the galvanic process, in particular after the preliminary nickel plating. The roughness values in direction transverse to the rolling direction were found to be higher than those in the longitudinal direction. Nevertheless, the roughness reduced slightly after electroplating, which results from a certain leveling effect through the electroplating process. Under the conditions cited above, layer thicknesses of 10 μm were attained for the nickel deposition and of 5 μm for the copper deposition.

The suspensions for EPD were prepared with the aid of an ultrasonic disintegrator. In so doing, the granulates were broken up, as TEM observation confirms (Fig. 3), sometimes to a primary particle size of around 45 nm.

The suspension for EPD was optimized regarding its electrostatic stability and suitability for electrophoretic deposition. The objective is to achieve as high a particle charge as possible. The influence of the particle charge on the migration rate of particles in EPD can be derived from the ζ potential, according to the universally recognized equation:

$$v_{el} = \frac{\zeta \cdot E_0 \cdot \varepsilon}{6 \cdot \pi \cdot \eta} \cdot f(\kappa \cdot a_0) \text{ with } \quad f(\kappa \cdot a_0) \in [1;\ 1,5]$$

where v_{el} Electrophoretically particle velocity, ε Dielectric constant, ζ Zeta potential, η Viscosity, E_0

Table 2 Roughness values of the substrate in direction transversal and longitudinal to the rolling direction

	X6Cr17 untreated	After preliminary nickel plating		Preliminary nickel plating + nickel sulfamate electrolyte		Preliminary nickel plating + acid copper electrolyte	
		Longitudinal	Transverse	Longitudinal	Transverse	Longitudinal	Transverse
R_a [μm]	0.03	0.49	0.61	0.35	0.45	0.25	0.51

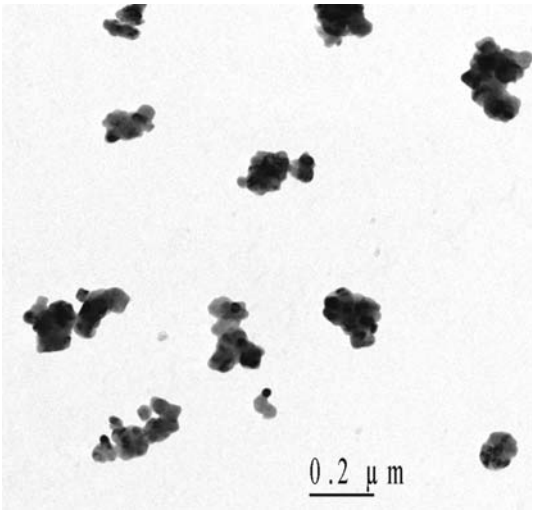

Fig. 3 TEM image of the ZrO_2 powder prepared ultrasonically

External electric field, κ Debey-Hückel parameter, a_0 Effective radius of the particle.

In this equation, which was derived by Smoluchowski and Hückel [11, 12], the ζ potential is the effective net charge of the particle in electrokinetic transport phenomena. The dependence of the stability of a suspension on the particle charge is usually explained by the DLVO theory [13]. The surface charge of particles were characterized using an Electrokinetic Sonic Analysis (ESA) System. In the present study, an ethanol ZrO_2 suspension with addition of 4-hydroxybenzoic acid was optimized. Figure 4 shows the measured values of ESA signal, which is related to the zeta potential, as function of 4-hydroxybenzoic acid concentration. These results were used to determine the ideal concentration of 4-hydroxybenzoic acid. A high particle charge of the same polarity also effects the electrostatic stability of a suspension and hence it also affects the coagulation and sedimentation behavior of the particles as well as the green density of the deposited layer.

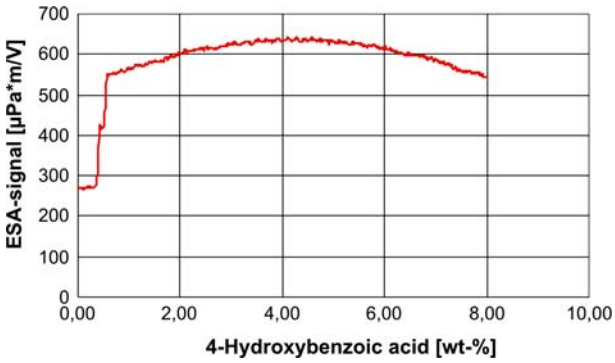

Fig. 4 ESA signal as a function of the concentration of 4-hydroxybenzoic acid for ethanolic dispersions of ZrO_2

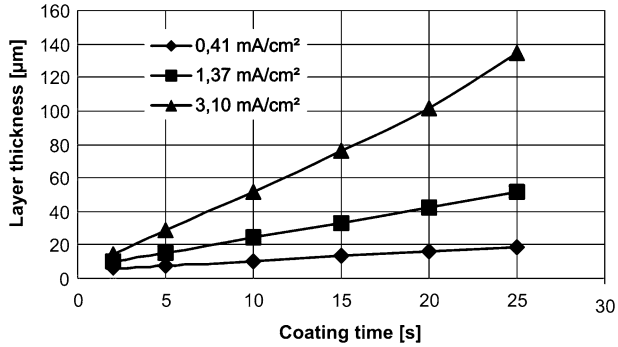

Fig. 5 Relation between coating time and ZrO_2 layer thickness achieved at various current densities

The ceramic layers were electrophoretically deposited on the metal surface using the optimized suspension. The layer thickness which can be attained depends on the current density and coating time. Figure 5 shows the relation between the layer thickness and the coating time for various current densities. It was demonstrated that thick ZrO_2 layers can be attained very effectively by means of electrophoresis.

The zirconium oxide layers produced electrophoretically were sintered in a vacuum (10^{-1} mbar) after drying at temperatures of 1150 °C for creating nickel–zirconium oxide layers and at 1050 °C for the copper–zirconium oxide layers. The porosity of the layers was determined to be 40–50%. The sintering in vacuum is necessary in order to prevent oxidation of the metal. An oxide layer would prevent contacting of the surface and hence it would impede the coating development both in electrophoretic layer production and in galvanic infiltration.

In the layers sintered at 1150 °C, an open-porous ceramic layer with clearly pronounced sintering necks resulted as shown in Fig. 6. As a result, the layer exhibits a high structural stability.

The sintering of the ceramic layer for production of the copper–zirconium oxide layers was carried out at significantly lower temperatures. The lower sintering temperature was necessary owing to the low melting point of copper. Formation of the sintering necks typical for the early stage of sintering cannot be observed at these low temperatures. However, it was assumed that the ceramic particles had already formed a fixed contact to one another as the layer did not separate from the substrate during the galvanic infiltration.

The sintering on a galvanic intermediate layer leads to a considerable improvement in the bonding of the ceramic layer onto the stainless steel, in contrast to earlier attempts in which the ceramic was applied directly onto the substrate and sintered [9]. A reason

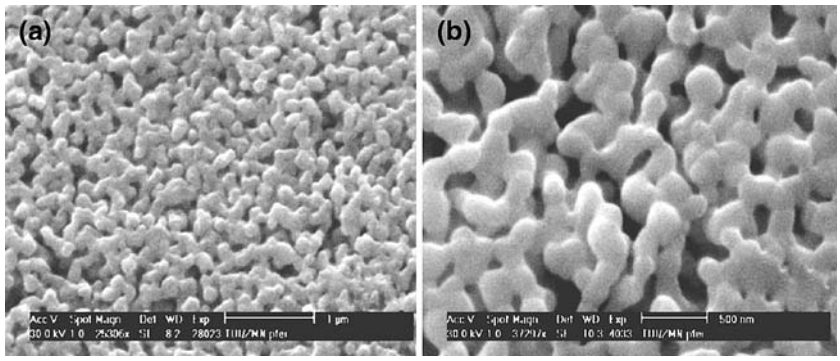

Fig. 6 SEM image of a zirconium oxide layer sintered at 1150 °C with homogenous open-porous structure (**a**) Overview, (**b**) Magnified

for this can be that, despite the use of a vacuum furnace for the sintering tests, the remaining oxygen in the vacuum chamber might here caused a minimum oxidation of the steel surface. The oxide layer prevents optimum adhesion of the ceramic layer after sintering. It also makes the contacting of the substrate more difficult for the galvanic infiltration of the porous ceramic layer. The use of a nickel or copper intermediate layer enabled this problem to be avoided. The galvanic intermediate layer therefore allowed an improved substrate adhesion of the ceramic layer.

Material transport through diffusion occurred between the substrate and the galvanic intermediate layer during sintering. At the same time, nickel or copper partially dissolves in the metal substrate. The remaining galvanic layer improves the contacting of the substrate during galvanic filling of the open-porous layer after sintering.

Nickel and copper were selected for the infiltration tests, as they exhibit a low brittleness in addition to good chemical and physical properties. The practical implementation of the galvanic filling did not present any problems despite the very narrow pore channels. The open porosity of the ZrO_2 layer could be completely filled. The metal extends through the ZrO_2 layer beginning from the substrate surface forming effectively an interpenetrating metal–ceramic compound layer.

Figure 7 shows an SEM image in BSE mode (material contrast image) of a sintered zirconium oxide layer, in which the metal infiltration with nickel was interrupted before nickel infiltration had reached the surface. The infiltration with metal, starting from the substrate and extending to the darker porous zirconium oxide layer, can be detected in the lower bright area. The uniform penetration of the metal into the pores is clearly discernible. This is also revealed by X-ray diffractometry measurements as well as energy-loss spectroscopy tests (EELS/TEM) on a sample

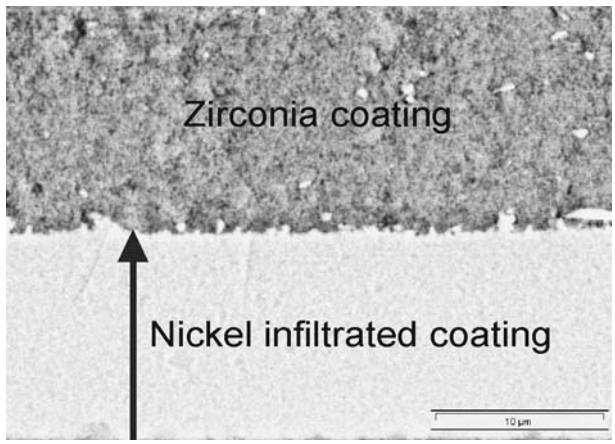

Fig. 7 Material contrast SEM image of a ceramic layer partially filled with nickel

prepared from the composite layer (Fig. 8a). By detecting the zirconium (Fig. 8b) as well as nickel (Fig. 8c) and their overlay (Fig. 8d) with the oxygen distribution examined at the same time, the EELS tests revealed the influence of nickel within the pores between the ceramic particles. The high-resolution determination of the lattice planes in the HRTEM images also demonstrates only ZrO_2 and nickel parameters.

In an extreme case, the process can be continued until nickel infiltration fills completely the ceramic layer and extends out of it, forming a metallic lustrous coating.

An improvement in the layer formation can be achieved through subsequent annealing in vacuum. In the process, the metal–ceramic composite layer combines with the primary galvanic intermediate layer. The final annealing process enables a strong material bonding of the composite layer with the substrate through reciprocal diffusion of the metal components. Figure 9 shows the cross section of sintered zirconium oxide layer, nickel-infiltrated at 1150 °C and finally

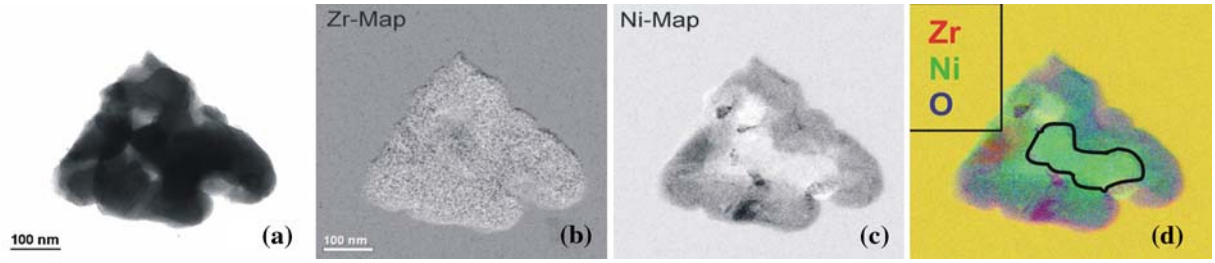

Fig. 8 Evidence of pore infiltration with nickel by means of EELS tests in the TEM

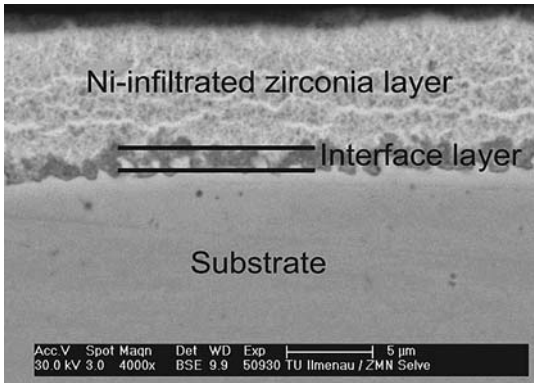

Fig. 9 Nickel–zirconium oxide composite layer with galvanic nickel intermediate (interface) layer on stainless steel substrate in backscattered electron (BSE) image after final annealing at 800 °C

annealed. The composite layer is firmly bonded to the metal substrate via the nickel intermediate layer.

Overlapping SEM images with EDX line scans, which represent the distribution of the individual elements in the transition zone from the substrate to the composite layer, revealed the distribution of the individual elements after heat treatment, shown for example in Fig. 10. In this figure, evaluation of the L-line is represented for the element zirconium, and evaluation of the K line of the spectrum for the elements nickel, chromium and iron.

It is clearly discernible that nickel has diffused very deeply into the metal substrate (Fig. 10a). This can consequently be explained by the fact that the nickel intermediate layer was already subjected to high temperatures for a very long period while sintering the ceramic, causing a very deep diffusion into the substrate. At the same time, chromium and iron from the stainless steel substrate diffused into the nickel layer. As Fig. 10b shows, it is interesting that both iron and chromium can even be detected in the composite layer after the final annealing. The concentration of these elements is found to be continous from the substrate into the composite layer. This thereby ensures a very strong material bonding of the composite layer to the substrate.

The same characteristics were observed when manufacturing the copper–zirconium oxide layers. Here too, copper already diffuses into the metal substrate while sintering the ceramic layer. Galvanic infiltration tests have revealed that the remaining copper intermediate layer is necessary for the subsequent galvanic filling of the porous ceramic. This ensures a better contacting of the substrate in the galvanic bath and hence a uniform penetration of the metal. After infiltration of the ceramic layer and subsequent thermal treatment at 800 °C, the metal diffusion is also discernible through EDX line scans for these samples, as shown in Fig. 11. In addition to the copper intermediate layer, Fig. 11a also reveals copper in the steel substrate. In the copper zirconium oxide composite layers, the EDX line scans in Fig. 11b show that both iron and chromium have diffused into this layer. These tests also allow the conclusion that the proportion of reciprocally diffused metal atoms is lower in

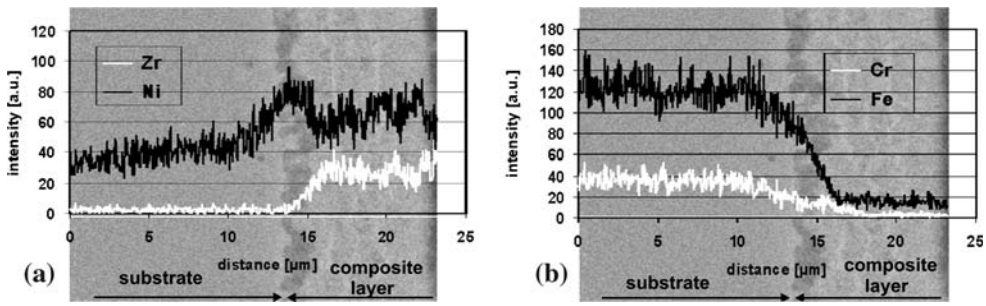

Fig. 10 EDX line scans with distribution of the elements over the sample cross-section for a ZrO_2/Ni system (**a**) Zirconium and nickel (**b**) Chromium and iron

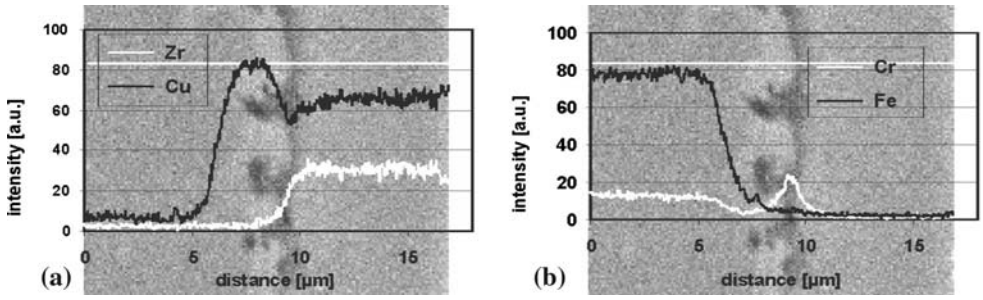

Fig. 11 EDX line scans with distribution of the elements over the sample cross-section for a ZrO_2/Cu system (**a**) Zirconium and copper (**b**)Chromium and iron

comparison to the nickel–zirconium oxide layers (Fig. 10). The significantly lower solubility of Fe and Cr from stainless steel in copper is to be cited as a reason for this, in addition to the lower temperature used during the sintering. Low contents of chromium and iron can also be detected in the composite layer. Nevertheless the tests confirm the strong bonding of the composite layer to the substrate as a consequence of the atomic interdiffusion observed.

Conclusions

The tests revealed that metal–ceramic composite layers on stainless steel can be produced through a combination of electrophoretic and electroplating technology, in which the properties of metal and ceramic can be advantageously combined. In the layers, metal and ceramic also penetrate over dimensions in the submicrometer range. This could be confirmed on both nickel–zirconium oxide layers and copper–zirconium oxide layers. Targeted thermal treatment processes made it possible to strongly bond the thesis the substrate through atomic diffusion processes. This opens up interesting areas of application for such coatings in wear and corrosion protection etc. as well as for high-temperature applications. The processes occurring can be explained with the accompanying solid-state physics analysis.

Acknowledgements The authors would like to thank Dr. (Engineering) K. Pfeifer and Graduate Chemist P. Mahr, Technical University of Ilmenau for some sample analyses and production of the composite layers. This work was supported financially by the Deutsche Forschungsgemeinschaft (reference KE 359/7-1). We thank Dr. A. R. Boccaccini (Imperial College London, UK) for his comments on the manuscript.

References

1. Burghardt W (1994) Galvanotechnik 85:406
2. Karayianni C, Vassiliou P (1998) J Mater Sci Lett 17:389
3. Maurin G, Barchichi CE (1999) in Proceedings of the 50. ISE Conference, p 284
4. Steinhäuser S, Wielage B, Grzybek A, Jakob Ch, Erler F, Nutsch R (2000) in Proceedings of the 197. Meeting of the Electrochemical Society, Inc., Toronto/Canada, 14.–18.05.2000
5. Put S, Vleugels J, Van der Biest O (2001) Scripta Mater 45:1139
6. Zhao SY, Chen S, Wang S, Quan Z (2000) J Colloid Interface Sci 221:161
7. Wang Z, Shemilt J, Xiao P (2000) Scripta Materialia 42:653
8. Shrestha NK, Sakurada K, Masuko M, Saji T (2001) Surf Coatings Technol 140:175
9. Kern H, Krüger HG, Schindler U, Knote A (2001) European Patent: PCT/EP02/10535, 20.09.2001
10. Krüger HG, Knote A, Schindler U, Kern H, Boccaccini AR (2004) J Mater Sci 39:839
11. Debye P, Hückel E (1923) Physik Zeitschrift 24:305
12. Henry DC (1931) Proc. Ref. Soc. Sev. London, p. 133ff
13. Verwey EJ, Th.J, Overbeek G (1948) Theory of stability of lyophobic colloids. Elsevier Publ. Comp., Amsterdam